J Solid State Electrochem (2010) 14:2121–2128
DOI 10.1007/s10008-010-1043-7

ORIGINAL PAPER

Investigations on current transients in porous alumina films during re-anodizing using the electrochemical quartz crystal microbalance

Adriana Ispas · Andreas Bund · Igor Vrublevsky

Received: 23 November 2009 / Revised: 25 February 2010 / Accepted: 3 March 2010 / Published online: 1 April 2010
© Springer-Verlag 2010

Abstract Current transients and mass variations in as-prepared and heat-treated anodic alumina films were measured during re-anodizing by means of voltammetry and electrochemical quartz crystal microbalance (EQCM), respectively. Aluminum electrodes (100 nm) on quartz crystals were prepared by thermal evaporation. Anodic alumina films were formed on the surface of Al electrodes in aqueous solutions of oxalic (0.3 M) and phosphoric (0.6 M) acid in the potentiostatic regime. The EQCM experiments did not detect an overshoot in the mass variation of the Al electrode during re-anodizing of heat-treated anodic alumina films. The observed current overshoot in transients proved the presence of electrons and electron holes injected from the contacts in the bulk of the oxide. This can be explained by the emergence of excess electrons in the barrier layer of the alumina films due to a change in the mobility of the electrons.

Keywords Electrochemical quartz crystal microbalance · Anodic alumina films · Current transient · Mobility · Oxalic acid · Phosphoric acid · Boric acid

A. Ispas · A. Bund
Physikalische Chemie und Elektrochemie,
Technische Universität Dresden,
01062 Dresden, Germany

I. Vrublevsky (✉)
Department of Micro and Nanoelectronics,
Belarusian State University of Informatics and Radioelectronics
Minsk,
220013 Minsk, Belarus
e-mail: vrublevsky@bsuir.edu.by

Introduction

Oxide growth on aluminum is determined by ionic conduction through the electronically insulating oxide film [1–4]. Numerous investigations have shown that the anodic current during anodization of Al in barrier-type electrolytes (e.g., neutral boric acid, ammonium borate, tartrate aqueous solutions, pH 5–7, [1, 5]) depends exponentially on the electric field in the oxide, according to the high field law. However, the ionic conduction emerges not immediately with perturbations of the applied current or potential but only after a certain relaxation period known as the transient process. Therefore, the behavior of anodic oxide films in electrochemical transient experiments cannot be explained in terms of the high field law. That is why various mechanisms of physical processes governing the transients in anodic oxide films such as relaxation of dielectric polarization [6], charge carrier generation [7], structural changes in the bulk [8], and build-up surface charge [9] were suggested in the literature. In [10], it was shown that the transient process is defined by a charge passed through the oxide film. Nevertheless, the nature of this charge remains unknown and requires new approaches for its investigation.

According to [11], during anodizing, the electrolyte not only provides oxygen ions for the oxidation but also injects electrons into the oxide conduction band. Such a suggestion has been made on the basis of a systematic study of the electrical breakdown of anodic oxide films as a function of temperature, concentration, composition of electrolyte, and anodic current density. As demonstrated in a number of investigations [11, 12], the high field strength in an anodic oxide film can accelerate such electrons to an energy sufficient to free other electrons through impact ionization

so that an avalanche multiplication and finally electric breakdown occurs.

The electronic component of conductivity does not contribute to the oxide film growth during anodizing [13]. Although this component is considerably smaller than the ionic component at steady-state anodizing, it may have a significant magnitude during transient processes.

The general problem during the investigation of anodic oxide growth is the separation of the underlying processes such as oxide growth related to the ionic transport and electron transfer reactions at the electrolyte/oxide interface [5, 14, 15]. The appearance of electrons at the solution/oxide interface is associated with the high electric field-induced ionization of water molecules yielding electrons, protons, and oxygen gas according to Eq. 1.

$$H_2O \rightarrow 1/2O_2 + 2H^+ + 2e^-. \quad (1)$$

The evolution of oxygen near the metal/oxide interface during anodizing of aluminum in various electrolytes was reported in [16–18]. The mechanism of field-induced ionization of water molecules releasing electrons was proposed in [19, 20]. Under the influence of the high electric field, electrons may be injected into the surface layer of the oxide, and they can be trapped in the electron traps generated by the presence of the electrolyte species or impurities incorporated from the anodizing bath. The existence of such trapped electrons was confirmed by luminescence and thermoluminescence measurements, whereas there were different hypotheses made about the nature of the traps for electrons, as shortly reviewed in [19]. One of the possible origins of the electrons traps is given in [19]. The incorporation of impurities from the electrolyte will induce a mechanical stress in the layer, which, at its turn, will produce defects. The traps for electrons can be related to these defects, while the trapped electrons will come from water dissociation [19].

Theoretical modeling has recently provided support for a movement of electrons and electron holes by hopping between trapping sites in valve metal oxides (e.g., hafnium oxide) at relatively high temperatures, while at low temperatures both electrons and electrons holes were identified as being stable immobile defects. However, very low activation energy is necessary for the electron migration process (ca. 0.01 eV), as it was proved by recent simulations, which took into account the temperature dependence [21]. The low activation energy could be caused by the transport of self-trapped electrons. These results suggest a possibility of relatively high mobility of trapped charges—electrons and electron holes [21]. Computer simulations also suggested that the mobility of ions is very low near the points where the oxide layers start to form and it is very high in the central part of the oxide film [22].

A very useful tool for surface science studies is the quartz crystal microbalance (QCM) method. This method is well established for thickness determination in the gas phase (evaporation rate monitor) and in liquids (plating rate monitor). With modern devices, mass detection of thin electrode surface layers with a resolution of 10 ng cm^{-2} can be readily achieved. In electrochemical experiments, QCM can be combined with electrochemical methods (e.g., voltammetry) that yield information about the total transferred electric charge (electrochemical quartz crystal microbalance, EQCM). Important information regarding the electroactive species can be obtained [23] with an EQCM, such as the molar mass [24] or the solvation number [25]. The method is based on the fact that the resonance frequency of a piezoelectric quartz crystal decreases by an amount Δf if a foreign mass Δm (in kg m^{-2}) is deposited on its surface [26] according to Eq. 2.

$$\Delta f = -2f_0^2/(\rho_Q \mu_Q)^{1/2} \Delta m \quad (2)$$

In Eq. 2, f_0 is the resonance frequency of the uncoated crystal, and ρ_Q and μ_Q are the density and shear modulus of quartz, respectively. Usually, flat disk-shaped quartz substrates are vacuum-coated with metal electrodes on both sides. One of these electrodes represents the working electrode and is exposed to the electrolyte. Anodization of an aluminum electrode increases its mass which is indicated by a decrease of the resonance frequency of the quartz crystal. If we assume that the net reaction is the oxidation of Al to Al_2O_3, we have a mass increase of 24 g mol^{-1} (1.5 mol of O) for the transference of 3 F electric charge. Thus, a plot of (F Δm) vs. Q (F is the Faraday constant and Q is in C m^{-2}) should have a slope of 8 g mol^{-1}. This figure is called the apparent molar mass, M_{app}, associated with the above oxidation reaction.

If part of the oxide dissolves via a chemical route, the experimental value of M_{app} will be lower than the theoretical value. Besides the mass increase due to oxide formation, there will be also a contribution due to liquid molecules that are trapped in the pores of the alumina layer. This effect will lead a higher value of M_{app} as it increases Δm without consuming electric charge. The viscous damping of the electrolyte also causes a frequency decrease that is proportional to the square root of the viscosity density product of the bathing solution [27]. In our case, this term represents a constant contribution to the overall frequency shift. As we are only discussing changes of the frequency during the anodization, the viscous damping term cancels out. It has been shown by Johannsmann et al. that a quartz crystal with a nano-porous alumina layer can be used to determine independently the density and viscosity of a liquid [28]. Similarly, it was shown that a thin mesoporous

TiO_2 film coated on a quartz crystal can be used to detect the density of liquids with unknown viscosity [29].

In the present paper, we wanted to study transient processes in porous alumina films under linear potential sweep conditions. Preliminary studies have shown that the conductivity of an annealed anodic alumina film returns to that of a freshly anodized film by further anodizing [30, 31]. Thus, we suggested that transient characteristics of annealed anodic films during repeated anodizing could give important information about the injection processes of charge carriers. To study these effects in detail, we used voltammetry combined with EQCM measurements. By using the EQCM technique, we got in situ information on the current densities and mass changes during anodizing/re-anodizing processes. Therefore, we could identify in situ the potential regions where the mass of the aluminum layer changes and where the oxide layer starts to growth. This in situ technique can complete the existing knowledge on the potentiodynamic behavior of as-grown and annealed alumina films, as presented in [10]. Moreover, this study enlarges the existing knowledge by analyzing the re-anodizing processes not only of alumina films grown in phosphoric acid, as in [10], but also of alumina films which were grown in oxalic acid.

Experimental

Blank quartz crystals (10 MHz AT-cut, 15-mm diameter) were purchased from Vectron International (Neckarbischofsheim, Germany). Two keyhole-patterned aluminum electrodes of 100-nm thickness and 5 mm diameter were thermally evaporated on the opposite faces of the quartz crystal through a mask using an evaporation device from Malz&Schmidt (Germany). The evaporation was done in vacuum at 10^{-4} Pa. The source of aluminum was an aluminum wire of 99.999% purity (Chempur). The aluminum evaporation was done from crucibles made of tungsten.

One of the aluminum electrodes (area of 0.22 cm^2) on the quartz crystal was used for anodizing (working electrode). A platinum plate or platinum net was used as the counter electrode during the anodization and re-anodization experiments, respectively. The reference electrode was a saturated calomel electrode (SCE, Sensortechnik Meinsberg GmbH, Germany). In the following, all potential values will be quoted with reference to the SCE.

Thin porous-type alumina films were prepared potentiostatically (at E=2 V for 300 s or at 7 V for 50 and 100 s) in oxalic acid (0.3 M, 18±0.1 °C) and in phosphoric acid (0.6 M, 18±0.1 °C). The solution was vigorously stirred during the anodizing process.

The re-anodizing experiments and, simultaneously, the EQCM measurements were carried out potentiodynamically at 50 mV s^{-1} in a barrier-type anodizing solution of 0.5 M H_3BO_3 and 0.05 M $Na_2B_4O_7$ (pH=7.3 at 22 °C) at room temperature. The electrochemical cell used for re-anodizing experiments was made of polytetrafluoroethylene. The quartz crystal was placed at the bottom of the cell and fixed between a Viton o-ring (solution side) and a silicone rubber gasket (air side).

A potentiostat model 263A from EG&G Instruments was used for anodizing and re-anodizing of Al films. A network analyzer model 5100A from Agilent was used in the EQCM experiments for determining the resonance frequency and the damping of the quartz crystal. The changes in the resonance frequency of the quartz crystal were in the order of some 10 Hz in the case of the re-anodizing experiments. The damping of the quartz crystal (measured as the half band width of the resonance curve) remained constant in all re-anodizing experiments. Therefore, one can use the Sauerbrey relation, Eq. 2, for the determination of the mass change from the frequency shift. It has been shown that Eq. 2 can be applied as long as the changes of the resonance frequency of the quartz crystal are much bigger (by some orders of magnitude) than the damping changes [32]. A scanning electron microscope (SEM) model DSM 982 from Zeiss Oberkochen, Germany, was used for investigating the morphology of the thin alumina layers.

The annealing of the samples, if indicated, was conducted in an ambient atmosphere for 1 hour at 200±5 °C. All the solutions in this study were prepared using distilled water, high-purity $(HOOC)_2$, H_3PO_4, H_3BO_3 acids, and sodium tetraborate, $Na_2B_4O_7$, purchased from Alfa Aesar.

The transient processes in porous oxide films on aluminum were studied during their re-anodizing. Two types of anodic alumina films were prepared for re-anodizing experiments: in one case the samples were heat-treated after the first anodizing process and in the second case the samples were further re-anodized in their state as-anodized, without any thermal treatment.

Results

Figure 1 shows micrographs of the top views of thin porous alumina films formed in oxalic and phosphoric acids. One can see that the diameter of the pores obtained potentiostatically at 7 V in 0.3 M $(HOOC)_2$ are smaller than 10 nm (Fig. 1a), whereas pores with a diameter of about 50 nm were obtained potentiostatically at 7 V in 0.6 M H_3PO_4 (Fig. 1b). The SEM investigations were conducted in order to evaluate the diameter of the pores formed in the two electrolytes studied here. As already discussed in the introductory section, when the pore diameter varies, the amount of trapped liquid in the working electrode will also

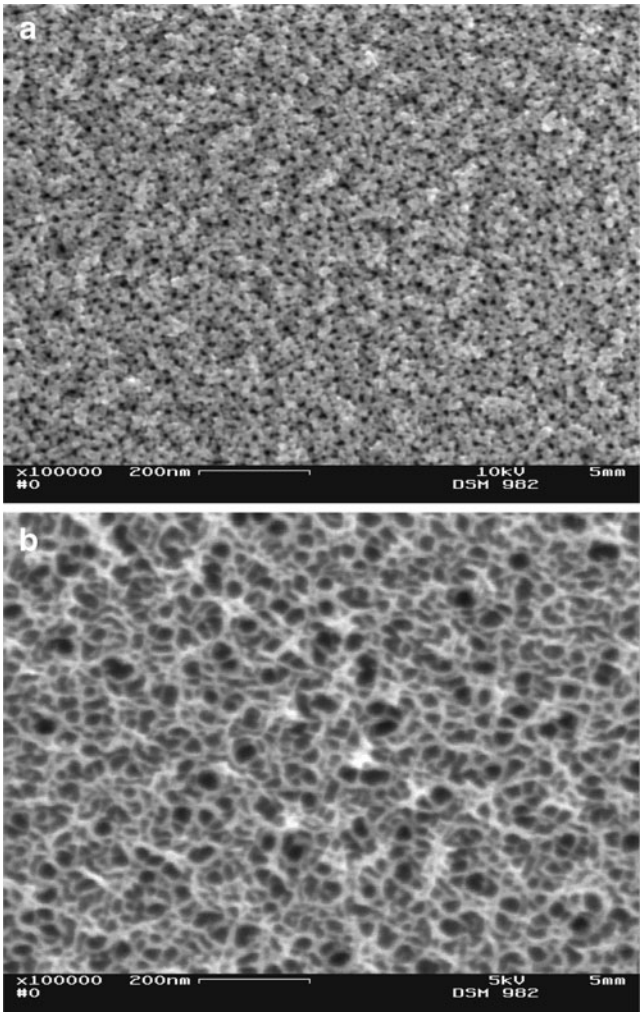

Fig. 1 Scanning electron micrographs of the oxide films potentiostatically grown at 7 V for 100 s in 0.3 M $(HOOC)_2$ (**a**) and at 7 V for 50 s in 0.6 M H_3PO_4 (**b**)

vary. The trapped liquid can contribute to changes of the resonance frequency and, in the end, of the calculated Δm (Eq. 2), which should be separated from the mass increase that is due to the growth of the oxide film.

Figure 2a shows a current–voltage curve for re-anodizing of heat-treated phosphoric acid alumina film in boric acid solution and the associated mass change. The mass variations were calculated from the EQCM data via Eq. 2 and they will be discussed below. An analogous curve for a heat-treated oxalic acid alumina film and the associated mass change is presented in Fig. 3. Figures 2a and 3a clearly demonstrate that there is a current overshoot in the transient during the re-anodizing of heat-treated anodic alumina films. One can also see that the mass does not start increasing simultaneously with current but with a small delay. The region of current increase without or with a very slightly mass increase will be denoted by *a* in the following. The region *b* is the region of the current overshoot and its further decay. Region *c* is a region of the steady-state film growth observed at a constant value of anodic current. The apparent molar masses for the data Figs. 2a and 3a are 5.7±0.2 g mol^{-1} and 5.8±0.7 g mol^{-1}, respectively (Figs. 2b and 3b). These apparent molar masses were calculated for the region *c*. As has been discussed above, these values of the apparent molar masses indicate that besides the formation of Al_2O_3 some dissolution reaction occurs. This can be either the (chemical) dissolution of alumina or the electrochemical formation of soluble Al species (e.g., hydrated Al^{3+}). Without an analysis of the solution composition (as performed, e.g., in [33]), it is not possible to discriminate between these two dissolution processes.

From Figs. 2a and 3a, one can calculate the slope that characterizes the mass increase as a function of the applied potential for the steady-state film growth region. A value of 0.106 µg cm^{-2} V^{-1} was obtained for this slope between 7.5 and 8.5 V for phosphoric acid alumina film and of 0.108 µg cm^{-2} V^{-1} between 7.7 and 8.5 V for oxalic acid alumina film.

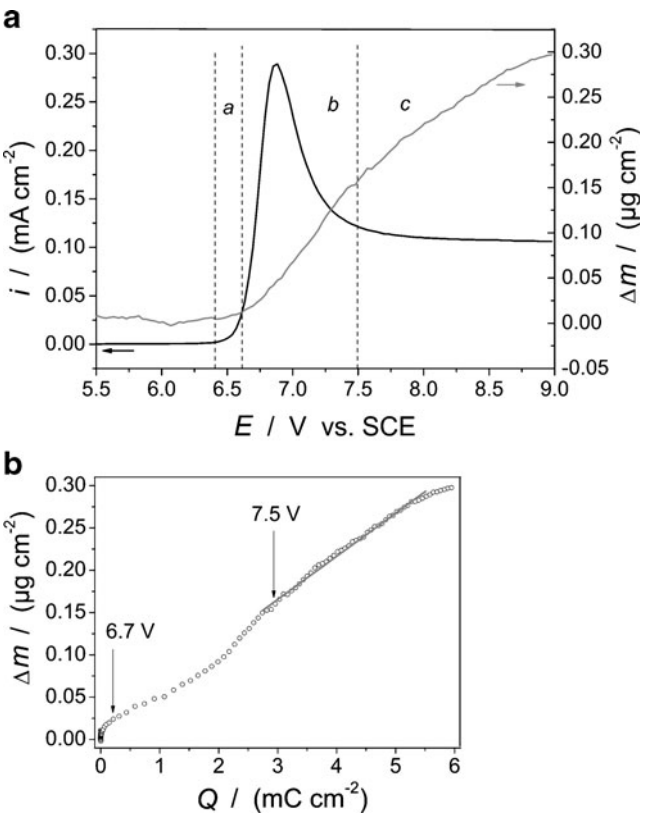

Fig. 2 **a** Re-anodization curve (50 mV s^{-1}, *black curve*) and the associated mass variations of heat-treated alumina film in boric acid solution (*grey curve*). The oxide film had been grown in phosphoric acid at 7 V for 50 s with a subsequent heat treatment at 200 °C for 1 h. **b** Mass vs. charge plot of the re-anodization curve shown in **a**. The slope of the line corresponds to an apparent molar mass of 5.7±0.2 g mol^{-1}

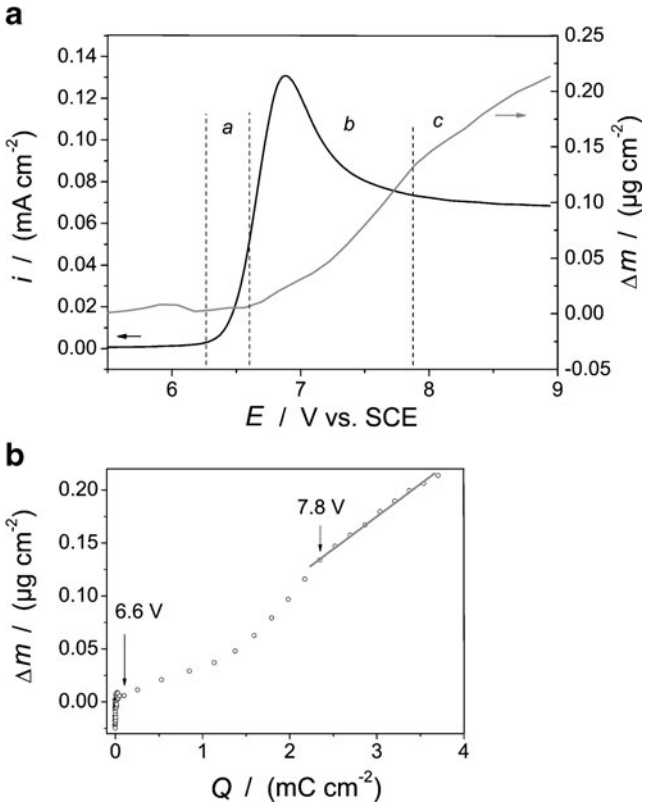

Fig. 3 **a** Re-anodization curve (50 mV s^{-1}, *black curve*) and associated mass variations (*grey curve*) of a heat-treated alumina film in boric acid solution. The film had been grown in oxalic acid at 7 V for 100 s with a subsequent heat treatment at 200 °C for 1 h. **b** Mass vs. charge plot of the re-anodization curve shown in **a**. The slope of the line corresponds to an apparent molar mass of 5.8±0.7 g mol^{-1}

Figure 4a shows a current–voltage curve for the re-anodization of as-prepared phosphoric acid alumina film in a boric acid solution and the associated mass change as determined by EQCM. An analogous curve for as-anodized oxalic acid alumina film and the associated mass change is presented in Fig. 5a. As in the case of the heat-treated anodic alumina films, we distinguish three typical regions in the current curves (Figs. 4a and 5a). The region *a* corresponds to the current increase without a significant mass change. The region *c* is a region of steady-state film growth and is characterized by a linear mass increase. Between region *a* and *c*, there is a transition region *b*. The apparent molar masses for the data in Figs. 4a and 5a are 5.7±0.2 and 3.4±0.3 g mol^{-1}, respectively (Figs. 4b and 5b). Again, there is a dissolution process occurring in parallel to the oxide growth. Interestingly, the dissolution at the initial moment of re-anodizing is stronger for the film prepared in oxalic acid (Fig. 5). The correlation coefficients of the fitted lines in Figs. 2b, 3b, 4b, and 5b with regard to the measured data points were between 0.9981 and 0.9994.

The growth rate in the steady-state film growth region can be calculated from Figs. 4a and 5a. It equals to 0.106 μg cm^{-2} V^{-1} between 2.5 and 3.4 V for phosphoric acid alumina film and 0.105 μg cm^{-2} V^{-1} between 2.5 and 3.4 V for oxalic acid alumina film.

The EQCM results in the region of steady-state film growth show that the growth rates of the anodic oxide during potentiodynamic re-anodization for as-prepared and heat-treated films are in the same order of magnitude. This is exactly what should be observed for electrolytes in which the anodic oxide dissolves only weakly, as the electrolyte used in the re-anodizing experiments in our present study. As numerous experiments show, there is a linear relationship between anodizing voltage and the oxide thickness in a barrier-type electrolyte [1, 34–36]. This fact indicates the permanent electric field strength in an anodic oxide film and implies that, for a potentiodynamic regime of re-anodizing with a constant sweep rate, the growth rates of new anodic oxide layers are constant for all films independent from their formation voltage.

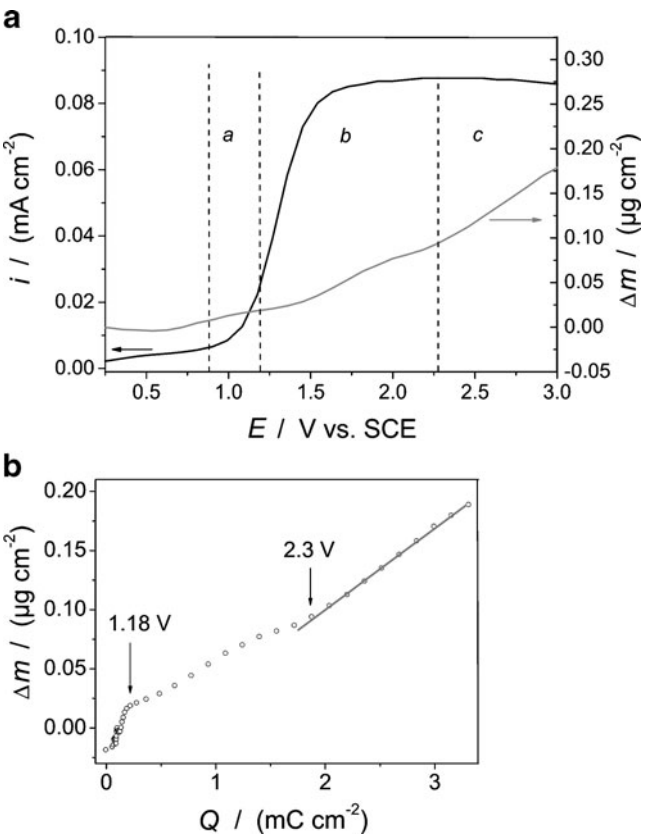

Fig. 4 **a** Re-anodization curve (50 mV s^{-1}, *black curve*) and associated mass variations (*grey curve*) of an as-prepared alumina film in boric acid solution. The film had been formed in phosphoric acid at 2 V for 300 s. **b** Mass vs. charge plot of the re-anodization curve shown in **a**. The slope of the line corresponds to an apparent molar mass of 5.7±0.2 g mol^{-1}

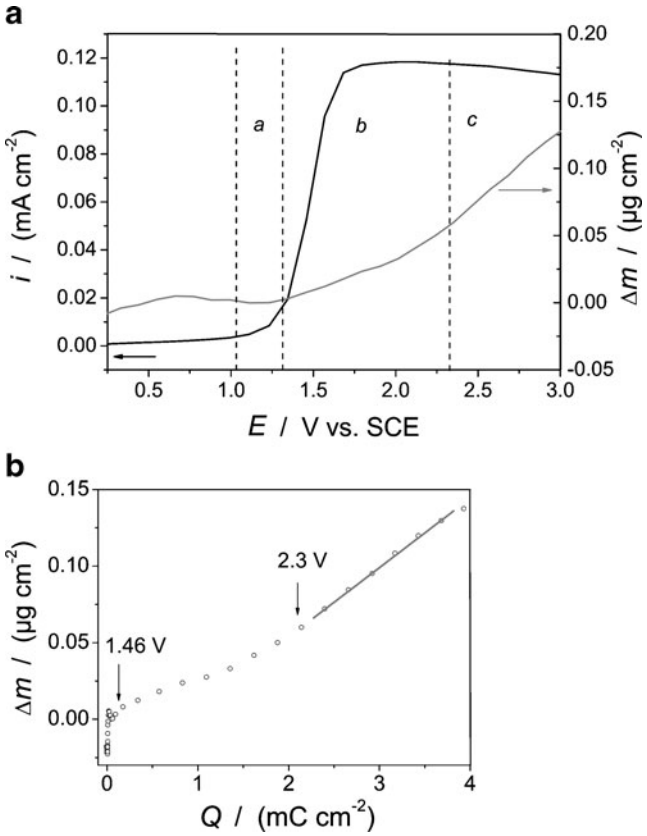

Fig. 5 **a** Re-anodization curve (50 mV s^{-1}, *black curve*) and associated mass variations (*grey curve*) of as-prepared alumina film in boric acid solution. The film had been formed in oxalic acid at 2 V for 300 s. **b** Mass vs. charge plot of the re-anodization curve shown in **a**. The slope of the line corresponds to an apparent molar mass of 3.4±0.3 g mol^{-1}

Discussion

The nature of current overshoot

It is known that the electronic conductivity of anodic alumina films is negligible [1]. However, at perturbations in applied potential, one can observe a significant electron current flow in a transient area [22]. As can be seen from Figs. 2 and 3, the region *a* of current growth is not accompanied by a significant mass change, so we can conclude that electron current is responsible for this region. The region of current growth (*b*) shows the injection of electrons and cation vacancies from the electrolyte/oxide interface and electron holes and anion vacancies from oxide/aluminum interface. It is followed by the region of current decay (*b*) showing the recombination of excess electrons and electron holes in the barrier layer. Therefore, with a decrease in electron component in the total current, the ionic component growths due to contribution of cation and anion vacancies injected from the contacts. The region *c* corresponds to a steady-state film growth accompanied by a linear growth of oxide mass. This indicates the permanent electric field in film during oxide growth.

The EQCM experiments did not detect an overshoot in the mass variation on the Al electrode during re-anodizing of heat-treated anodic alumina films. Therefore, the observed current overshoot in transients can be explained only by the presence of electrons and electron holes—typical point defects injected from the contacts in the bulk of oxide. Thus, these results confirm the assumption of the Macdonald model describing the formation of the oxide films on the basis of existence of many point defects in the layers such as cation vacancies, anion vacancies, electrons, or electron holes [37–39].

Peculiarities of electron current flow in an insulator containing electron traps

The presence of empty electron traps in an insulator results in a considerable decrease of electronic current. Electron traps, which are initially empty, trap a part of the injected electrons from the electrolyte contact and thus do not allow their movement in an electric field. Therefore, the amount of free electrons in the conduction band and the current, respectively, decreases. There is also another important effect linked with the movement of electrons under the high electric field. It is a slowdown in the mobility of electrons, and decrease in electron lifetime correspondingly, due to a capture of electrons by traps.

To explain the emergence of excess electrons in the barrier layer of anodic oxide, we will use the approach proposed in [10] for the electron current flow in an insulator containing electron traps.

Figure 6 presents a typical electronic current–voltage curve with different regions for the insulator with electron traps according to [40]. Such an electronic current–voltage characteristic consists of three regions: the first one with

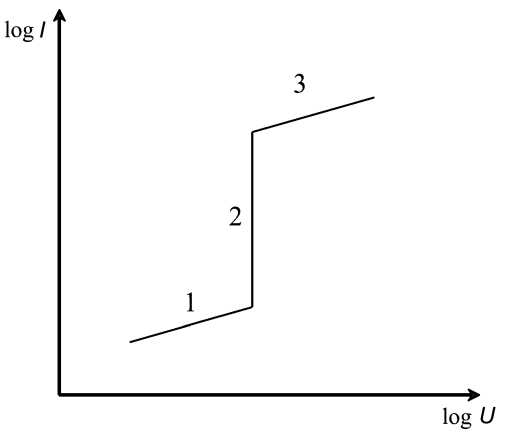

Fig. 6 Typical electronic current–voltage curve for the insulator with electron traps according to [40]

low current is a region determined by electron traps, the second region—a region of a sharp current growth (complete filling of electron traps), and the last one with high current—a region corresponding to the current in an insulator without traps. In other words, when all traps are filled, the amount of electrons in the barrier layer grows stepwise and, as a consequence, the electronic current jumps.

It is worth noticing that, when all electron traps are filled and the electron lifetime in oxide conduction band increases sharply, the mobility of electrons should increase stepwise (what would result in emergence of excess electrons in the barrier layer).

Current overshoots in heat-treated anodic alumina films

It is obvious that the current peak in the transient corresponds to the maximum number of charges injected from the contacts into the bulk of alumina barrier layer. After reaching its maximum, the current decreases because the excess electrons are leaving the barrier layer and then a current decay turns into a saturation region (Figs. 2a and 3a). As shown in [10], the current overshoot in heat-treated anodic alumina films can be characterized by the amount of charge passed. Heat treatment at 200 °C modifies the conductive properties of the anodic oxide films by reducing the number of the electron traps and by emptying the electron traps that remained. It was shown that annealing increases the oxide density by decreasing the numbers of defects in the oxide film and by desorption of the small water quantity that could have been incorporated in the oxide film [19].

The emergence of excess electrons in the barrier layer of heat-treated porous films during re-anodizing is connected with the change in mobility of electrons. After heat treatment of anodic films, electron traps in the bulk of oxide are empty. Some injected electrons in the barrier layer of a heat-treated film are trapped by empty electron traps. This decreases the free path of electrons. In this case, the migration of electrons is characterized by the low mobility. After all electron traps in the barrier layer are filled, electrons possess higher mobilities as nothing restricts their movement. In this case, the same value of electronic current can be provided by a smaller amount of electrons. That is why extra electrons become excess in the barrier layer of anodic alumina.

It is obvious that an as-anodized film in which all electron traps are filled has a high mobility of electrons in the barrier layer. That is why there is no current overshoot observed during re-anodizing of such films [10]. In case of heat-treated porous alumina films, electrons in the barrier layer initially have low mobility.

We should point out that electroluminescence is also observed during Al anodizing [41–43]. This is a direct evidence of the migration of electrons and electron holes in anodic oxide and their further recombination.

EQCM tests

EQCM data were recorded during the first anodizing of aluminum layers at 2 V for 300 s in both electrolytes (0.3 M $(HOOC)_2$ and 0.6 M H_3PO_4). An increase of the resonance frequency of the quartz crystal with ca. 1,300 Hz was obtained in the case that phosphoric acid was used (not shown). The changes in the full width of half maximum (FWHM) of the resonance curve were in this case in the order of ca. 300 Hz. As the changes of the resonance frequency are much bigger than the changes in the FWHM, one can apply the Sauerbrey equation to quantify the amount of dissolved mass [32]. Thus, approximately 6 μg cm^{-2} from the aluminum was dissolved during the first anodizing in H_3PO_4, which corresponds to ca. 23 nm. In the case that the oxalic acid was used, the changes of the resonance frequency were in the same order of magnitude as the changes in the FWHM during the first anodizing step (not shown). Therefore, one cannot quantify how much of the aluminum was dissolved in this case by applying the Sauerbrey equation. These results are in agreement with the dimensions of the pores obtained in the two electrolytes (Fig. 1). Thus, much more of the aluminum electrode is dissolved in H_3PO_4 in comparison to the mass dissolved in $(HOOC)_2$ under similar conditions during the first anodizing step.

An increase of mass of ca. 0.20 μg cm^{-2} was noticed during re-anodizing of alumina layers obtained in both H_3PO_4 and $(HOOC)_2$ solutions. The mass increase was almost the same for the alumina layers re-anodized after an annealing treatment or without any heat treatment. As mentioned above, the mass increase did not occur exactly with the current increase, but with some delay. Such a delay between the mass increase and the current increase has also been reported by Zhang and Devine, who used EQCM during the potentiodynamically anodizing of aluminum layers [44]. They concluded that the current which is not associated with the film formation can come from some non-film-forming oxidation reactions, like the oxidation of solvent and/or anion [44]. However, as previously mentioned ("The nature of current overshoot" section), one can attribute this current to electrons injected from the electrolyte into the surface oxide layer.

Conclusions

The combination of the EQCM method with voltammetry allowed us to explain the nature of the current overshoot

observed in transients during re-anodizing of heat-treated anodic alumina films.

The EQCM experiments did not detect an overshoot in the mass variation on the Al electrode during re-anodizing of heat-treated anodic alumina films. Therefore, the observed current overshoot in transients supports the presence of excess electrons and electron holes—typical point defects injected from the contacts in the bulk of oxide.

The results of EQCM on the region of steady-state film growth showed that the mass variation during potentiodynamic re-anodization (50 mV s^{-1}) in a barrier-type electrolyte of 0.5 M H_3BO_3 and 0.05 M $Na_2B_4O_7$ was the same for as-prepared and heat-treated anodic alumina films and equaled to 0.106±0.002 μg cm^{-2} V^{-1}.

It was shown that current overshoot in transient for heat-treated films can be explained by the emergence of excess electrons in the barrier layer as a result of change in the field mobility of electrons.

Acknowledgements The authors are grateful to the Deutsche Forschungsgemeinschaft (Germany) within the Grant BU 1200/16-1 for the financial support of this work.

References

1. Diggle JW, Downie TC, Goulding CW (1969) Chem Rev 69: 365–405
2. Patermarakis G (2009) J Electroanal Chem 635:39–50
3. Patermarakis G, Moussoutzanis K, Chandrinos J (2001) J Solid State Electrochem 6:39–54
4. Patermarakis G, Chandrinos J, Masavetas K (2007) J Solid State Electrochem 11:1191–1204
5. Thompson GE, Xu Y, Skeldon P, Shimizu K, Han SH, Wood GC (1987) Phil Mag B55:651–667
6. Dignam MJ (1972) In: Diggle JW (ed) Oxides and oxide films 1. New York, Marcel Dekker
7. Bean CP, Fisher JC, Vermilyea DA (1956) Phys Rev 101:551–554
8. Young L, Smith DJ (1979) J Electrochem Soc 126:765–768
9. De Wit HJ, Wijenberg C, Crevecoeur C (1979) J Electrochem Soc 126:779–785
10. Vrublevsky I, Jagminas A, Schreckenbach J, Goedel WA (2008) Solid State Sci 10:1605–1611
11. Ikonopisov S (1977) Electrochim Acta 22:1077–1082
12. Albella JM, Montero I, Martinez-Duart JM (1987) Electrochim Acta 32:255–258
13. Patermarakis G, Karayianni H, Masavetas K, Chandrinos J (2009) J Solid State Electrochem 13:1831–1847
14. Patermarakis G, Moussoutzanis K, Nikolopoulos N (1999) J Solid State Electrochem 3:193–204
15. Patermarakis G (2006) J Solid State Electrochem 10:211–222
16. Zhu XF, Li DD, Song Y, Xiao YH (2005) Matter Lett 59: 3160–3163
17. Shimizu K, Habazaki H, Skeldon P (2002) Electrochim Acta 47:1225–1228
18. Zhuravlyova E, Iglesias-Rubianes L, Pakes A, Skeldon P, Thompson GE, Zhou X, Quance T, Graham MJ, Habazaki H, Shimizu K (2002) Corros Sci 44:2153–2159
19. Lambert J, Guthmann C, Ortega C, Saint-Jean M (2002) Appl Phys 91:9161–9169
20. Lyuksyutov SF, Paramonov PB, Dolog I, Ralich RM (2003) Nanotechnol 14:716–721
21. Munoz Ramo D, Shluger AL, Gavartin JL, Bersuker G (2007) Phys Rev Lett 99:155504
22. Lohrengel MM (1993) Mater Sci Eng R11:243–294
23. Bund A, Schwitzgebel G (2000) Electrochim Acta 45:3703–3710
24. Bund A, Schneider O, Dehnke V (2002) Phys Chem Chem Phys 4:3552–3554
25. Bund A, Neudeck S (2004) J Phys Chem B108:17845–17850
26. Sauerbrey G (1959) Z Phys 155:206–222
27. Kanazawa KK, Gordon JG II (1985) Anal Chim Acta 175:99–105
28. Goubaidoulline I, Reuber J, Merz F, Johannsmann D (2005) J Appl Phys 98:014305
29. Schoen P, Michalek R, Walder L (1999) Anal Chem 71:3305–3310
30. Vrublevsky I, Jagminas A, Schreckenbach J, Goedel WA (2007) Electrochim Acta 53:300–304
31. Vrublevsky I, Parkoun V, Schreckenbach J, Goedel WA (2006) Appl Surf Sci 252:5100–5108
32. Bund A, Schneider M (2002) J Electrochem Soc 149:E331–E339
33. Naoi K, Oura Y, Ue M (1997) Denki Kagaku 65:1066–1069
34. Young L (1961) Anodic oxide films. Academic, London
35. Shimizu K, Thompson GE, Wood GC (1981) Thin Solid Films 81:39–44
36. Ikonopisov S, Andreeva L, Vodenicharov C (1970) Electrochim Acta 15:421–429
37. Chao CY, Lin LF, Macdonald DD (1981) J Electrochem Soc 128:1187–1194
38. Lin LF, Chao CY, Macdonald DD (1981) J Electrochem Soc 128:1194–1198
39. Macdonald DD, Urquidi-Macdonald M (1990) J Electrochem Soc 137:2395–2402
40. Maissel L (1970) In: Maissel L, Glang R (eds) Handbook of thin film technology. New York, McGraw-Hill
41. Belca I, Kasalica B (1999) Zekovic Lj, Jovanic B, Vasilic R. Electochim Acta 45:993–996
42. Stojadinovic S, Tadic M, Belca I, Kasalica B, Zekovic LJ (2007) Electrochim Acta 52:7166–7170
43. Stojadinovic S, Belca I, Kasalica B, Zekovic LJ, Tadic M (2006) Electrochem Commun 8:1621–1624
44. Zhang X, Devine TM (2006) J Electrochem Soc 153: B344–B351